Chapter 4

Prediction of Structure and Antagonist Binding Site:

Mouse CCR1

Abstract

In this chapter we describe the prediction of structure and the antagonist binding site for the mouse chemokine receptor 1 (mCCR1) using MembStruk v4.0. Preliminary function prediction was achieved via the HierDock protocol, used to dock a set of three ligands. The well-known antagonist BX471 binds between transmembrane (TM) helices 2-7, with a lower binding energy than the other two antagonists. With the exception of two residues, the residues in the 5Å binding site of BX471 are identical in both human and mCCR1. Compared to the predicted binding site of BX471 in human CCR1, we find that Tyr113 (TM3) is not nearly as critical for ligand recognition. Instead, the rotation of TM3 is such that Tyr114 now faces the binding cavity, contributing more favorably to the binding energy. Detailed analysis of the binding energy contributions of such conserved residues shows the importance of helical rotations in explaining binding differentials across homologous receptors.

Additionally, mutations in the mCCR1 binding site (e.g. Gly168 to Ala168 in TM4) result in significantly weaker interactions with the functional groups of BX471. The highly conserved (across most chemokine receptors) TM7 residue Glu287 interacts strongly with the ligand piperazine functionality, a binding motif which is consistent with previously published data. Furthermore, our calculated binding energies agree well with the trend in experimental binding affinities. Thus, this study provides the necessary framework for complete structural validation through docking of larger antagonist libraries.

Introduction

Chemokine receptors are important drug targets for auto-immune disorders[1-3]. Since the chemokine receptors are diverse across many organisms, one of the major challenges in drug design for these receptors is validating an animal model that shows a drug response similar to that seen in human models. For instance, BX471 is a potent antagonist for hCCR1 that shows poor binding affinity to mouse CCR1 (mCCR1)[4]. This is especially surprising considering the sequence identity (79%) between human and mCCR1. In earlier work we attempted to predict the differential binding affinity of BX471 (between mCCR1 and hCCR1) using a structure of mCCR1 homology modeled from our calculated hCCR1 model. This analysis showed that BX471 bound better to mCCR1 than hCCR1, failing to properly account for the differential binding. Therefore we predicted the mCCR1 structure using MembStruk[5-7]. We further validated this structure by predicting the binding sites of three antagonists using the HierDock method[6,8-9]. In this chapter we present the details of the predicted mCCR1 structure and the ligand binding site.

Computational Methods

Structure Prediction

MembStruk v4.0 was used to predict the structure of mCCR1. The general procedure has already been described for hCCR1 (Chapter 2), although differences for mCCR1 will be discussed below.

I. Transmembrane (TM) region prediction for mCCR1

The same set of sequences that was used for hCCR1 was also used for generating the multiple sequence alignment for mCCR1 TM region prediction. The seven predicted TM regions were located in identical regions in both human and mCCR1 sequences. The TM2ndS program was used to calculate a complete hydrophobicity profile for mCCR1, shown in Figure 4-2. Average hydrophobicity values of the sequence (without the C and N termini) are used to determine a threshold baseline, used to identify the TM domains (Figure 4-3).

II. TM bundle assembly and optimization of helical translation and rotation

Compared to hCCR1, the hydrophobic centers for mCCR1 are only different by one residue in TM 1. The center is Val49 for mCCR1 whereas it is Val50 for hCCR1. There are a total of 34 mutations in the TM regions, broken down as follows: TM1 (8), TM2 (3), TM3 (2), TM4 (4), TM5 (5), TM6 (9), and TM7 (3). It is interesting to note that

these TM mutations are anywhere from 2-10 residues away from either side of the hydrophobic center.

Each helix is translated to fit the hydrophobic centers to a plane, and rotations optimized via net hydrophobic moment reorientation for TMs 1-2, and 4-7. Figures 4-4 and 4-5 show these moments before and after rotation, respectively. Rotational orientation optimization over a finer grid of rotation angles (-30° to +30°) was done using the RotMin procedure. To identify alternate low energy conformations for the bundle, we rotated each helix through a grid of angles (360° in 5° increments) for the main chain, reassigning side chains, and minimizing the potential energy yields an energy scan profile (Figure 4-6) with the initial structure represented at 0°. Therefore, the initial conformation was used for subsequent optimization.

Results and Discussion

Description of the mCCR1 Structure and Comparison to hCCR1

Location of Conserved Residues and Comparison to BR and hCCR1

Many polar inter-helical interactions are observed in the predicted mCCR1 structure. Figure 4-9 shows a water mediated salt bridge between Lys94 (TM2) and Glu287 (TM7). The interaction is not bidentate (unlike hCCR1), and analysis of the helical rotations shows that TM3 of mCCR1 is in fact rotated away from this face of TM2. However, a bidentate salt bridge is seen between Glu120 (TM3) and His293 (TM7), with distances of 3.72 and 5.82 Å (Figure 4-10). Such interactions between Glu122 (TM3) and His211 (TM5) have been observed in BR, and in our hCCR1 structure (albeit at shorter distances). There is also hydrogen bonding between the very highly conserved residues (across many GPCRs) Asp80 (TM2) and Asn297 (TM7). The distances reflected in Figure 4-11 are suggestive of water mediation, as in BR[10].

As shown in Figure 4-12, the mCCR1 corollary to the conserved TM6 WXPFF motif in biogenic amines[11] is WTPYN, of which Asn256 (TM6) hydrogen bonds to Tyr113 (TM3) and Tyr114 (TM3). Analysis of similar interactions in hCCR1 did not show contribution from Tyr114, presumably because this side chain is facing TM4. Figure 4-13 shows Asn75 (TM2) hydrogen bonding with the most conserved TM4 residue, Trp158. Comparing to the crystal structure of BR, it is evident that there is a hydrogen bond between this Asn on TM2 and a Trp on TM4.

The mCCR1 has 18% overall sequence identity to BR, and 22% in the TM region. The main chain RMSD is 5.20 Å, and an overlay of the two structures is shown in Figure 4-14. These values are similar to what we calculated between hCCR1 and BR, and Figure 4-15 rationalizes this by illustrating the similarity between hCCR1 and mCCR1 (RMSD of 2.91 Å).

It is interesting to note that the bends in Figure 4-15 occur in seemingly identical locations on each helix, suggesting that helix breakers are conserved. Analysis of the sequence alignment for these two receptors shows 83% sequence identity in the TM regions; 79% overall (Figure 4-16). Furthermore, every TM proline residue is indeed conserved across these receptors (and by association, BR): Pro38 (TM1), Pro39 (TM1), Pro88 (TM2), Pro167 (TM4), Pro211 (TM5), Pro254 (TM6), and Pro298 (TM7). As before, comparison to BR shows that there are three conserved prolines that also cause similar bends: Pro170 (TM4), Pro215 (TM5), and Pro267 (TM7). Provided in Table 4-1 are both the tilt and bend angles for TMs 1-7.

Results on Antagonist Binding Site Predictions for mCCR1

mCCR1 function prediction is accomplished by predicting ligand binding sites and trends in binding energies for a series of antagonists using the validated HierDock procedure. The procedure is again very similar to that described for hCCR1 in Chapter 2.

Binding site determination via coarse-grain docking

A total of 11625 spheres partitioned over 49 $(10Å)^3$ boxes were obtained for mCCR1 (Figure 4-7). After excluding binding regions in the loops and EC/IC boundaries, DOCK[12] was used to perform coarse-grain docking in each box. The best conformations in each box are hierarchically scored, yielding a total of 195 spheres merged from regions 27, 31, and 32 (Figure 4-8).

Predicted Binding Sites of Antagonists

In this study we docked three ligands: BX523 (quaternary ammonium salt), BX511, and BX471[13] (Figure 4-17). The pK_a values (calculated using quantum mechanics) for BX511 (4.3) and 471 (5.7) indicated that these species were not protonated (at the piperadinyl and piperazinyl nitrogens) at physiological pH, and so the neutral species were docked. BX523 and BX511 have similar structural backbones, although the bridging alkyl linker is one carbon longer in BX511.

Predicted Binding Site for BX523 (K_i = 52 nM)

The 5 Å binding cavity spans TMs 1, 2, 3, 4, 6, and 7 (Figure 4-18). The most dominant Coulombic contributions are from Ser110 (TM3) and Glu287 (TM3). These interactions are with the positively charged quarternary amine group on the piperidine ring, and thus very strongly coupled. The chlorine substituted aromatic ring weakly

hydrogen bonds with Tyr118 (TM3). This weak interaction could be due in part to the side chain placement of Tyr114 (TM4), which clearly repels the hydroxy substituent on the piperidine ring. There are also a number of favorable pi-pi aromatic stacking interactions, such as that between Phe260 (TM6) and the chlorine substituted aromatic ring. Another example of this is between Trp90 (TM2), Trp99 (TM2), and the ligand phenyl ring, which stacks directly beneath the plane of these tryptophans. Additionally, a weaker sigma-pi type interaction is observed between Tyr41 (TM1) and one of the unsubstituted phenyl rings on the ligand.

Finally, only 86% of the binding energy is recovered from interactions with the residues in the binding cavity (within 5 Å of the ligand), with an additional 10% attributable to desolvation (Figure 4-3). This data is indicative of an initial ligand conformation that is strained. Inspection of the geometry in fact shows a C-C-C angle of 108.9° (opposite the nitrogen atom in the piperidine ring), compared to an experimental angle of 113° obtained from a crystal structure of a model compound[14]. For future work, it is instructive to note that sampling the full conformational space of this ligand in solution seems necessary. This can be accomplished by docking to the receptor a large ensemble of diverse ligand conformations generated outside of the protein (using a grid or Monte Carlo approach).

Predicted Binding Site for BX511 (K_i = 332 nM)

As shown in Figure 4-19, the BX511 binding site involves contributions from TMs 2-7. As with BX523, we similarly observe the effects of Ser110 (TM3) and Glu287

(TM7) in the binding site. However, the ligand seems to have shifted further away from Ser110 (TM3), perhaps because of the larger size of BX511 compared to BX523. This ligand also features a cyano functionality, which may interact long-range (7.96 Å) with Ser110 (TM3). The stacking interaction with Trp90 (TM2) and Trp99 (TM2) is conserved, along with the pi-pi stacking with Phe260 (TM6).

One notable difference is that Tyr118 (TM3) is just outside of the binding cavity, so in this bound conformation hydrogen bonding with Asn204 (TM5) is likely (similar to what we observed in the case of some hCCR1 antagonists). Since the ligand is shifted closer to TMs 1, 2, and 7 than BX523, the repulsive character of Tyr114 (TM3) is diminished by 1.2 kcal/mol. Summation of the cavity and solvation energies returns 97% of the calculated binding energy, although the solvation contribution (13%) is larger than what we observe for hCCR1 antagonists. As outlined above in the BX523 section, this is primarily due to the ligand internal strain energy, and will be addressed in subsequent studies.

Predicted Binding Site for BX471 (K_i = 380 nM) and Comparison to hCCR1

The binding domain of BX471 in mCCR1 involves contributions from TMs 2-7. Figure 4-20 shows a number of key interactions thought to be important in stabilizing the bound conformation of BX471. The chlorine substituted aromatic ring is anchored by Tyr118 (TM3) at a distance of 3.66 Å. The urea hydrogens are interacting with the oxygen atom on Tyr114 (TM3), while the adjacent carbonyl couples to Ala168 (TM4). The ester moiety likely hydrogen bonds with the terminal hydrogen of Tyr114 (TM3),

unlike the interaction with Ser110 (TM3) we observed in hCCR1. Finally, the fluorine substituted aromatic hydrogen bonds with Tyr291 (TM7) at a distance of 4.72 Å. This distance is larger than what we observed previously for hCCR1 (3.87 Å), indicating a weaker degree of coupling due to a tilt in ligand conformation or difference in TM7 rotation.

Shown in Table 4-2 are the FF energies for these interactions (5Å binding cavity), decomposed by hydrophobic and ionic contributions. The residues in blue interact in ways that are more favorable in mCCR1 than hCCR1, while the ones in red are less favorable in energy. It is evident that Tyr113 has diminished greatly in stabilization energy, due to the fact that in mCCR1 the rotation of TM3 orients this side chain away from the binding pocket. This is somewhat compensated for by the fact that the rotation of TM3 in mCCR1 allows Tyr114 to face and pack favorably around the ligand, while this is not the case in hCCR1. Furthermore, Ser110 in mCCR1 is now hardly contributing to ligand binding, primarily because the ligand has also changed orientation in the binding cavity. This data indicates that subtle TM rotations are the key to rationalizing binding differentials between highly homologous structures.

Two features differentiating hCCR1 and mCCR1 in this cavity are Ala168 (TM4) and Phe260 (TM6) in mCCR1. These residues are mutated from the human structure, where they are Gly168 (TM4) and Leu260 (TM6), respectively. Although the energies indicate that the interaction of Phe260 is quite strong in terms of hydrophobic packing, repulsive character is clearly introduced in this mutation. A large component of this stabilization stems from stacking with the chlorine substituted aromatic ring. On the other hand, going from Gly to Ala lowers the BE by 4.5 kcal/mol, almost completely in

Coulombic contributions. At this stage, it is not entirely clear why a subtle change in side chain placement would affect such a change in energy. Finally, 97% of the binding energy is recovered by summing the cavity and solvation energies.

Antagonist Binding Site Comparison to Homology Model Results

Onuffer et al. built a homology model of hCCR1[4] based on the crystal structure of bovine rhodopsin. To this structure they manually docked the antagonist BX510, which differs from BX511 (Figure 4-17) only in that it has a three carbon alkyl linker (BX511 has a four unit chain). Compared to Figure 4-21, our result differs mainly in that the binding mode of the ligand is inverted in the cavity, which actually contains many of the same residues (mapped to the mouse structure). The common feature is of course the interaction of the hydroxypiperizine ring with Glu287 (TM7), at a distance of 5.1 Å in their model, compared to 4.80 Å in our BX511 binding site. This corollary can also be drawn to the quaternary ammonium salt ligand BX523, which they contend would couple much stronger to Glu287 (TM7). Of particular interest is the fact that Glu287 (TM7) is conserved across the chemokine receptor family. No specific insight is provided into the hCCR1 to mCCR1 Leu260 to Phe260 (TM7) mutation, although it can be inferred (based on their binding mode) that the steric bulk of this substitution would seriously disrupt the binding mode and thus lower binding affinity for mCCR1.

Conclusions

We have constructed a structural model of mCCR1 using MembStruk v4.0. The stability of the receptor was assessed by analysis of stabilizing interhelical interactions, many of which are conserved in BR and hCCR1. Further comparison to hCCR1 elucidated the importance of subtle differences in helical rotation across such highly homologous receptors. The HierDock protocol was then used to determine the antagonist binding site in mCCR1. A set of three ligands with known binding affinities were docked to this region, and binding energies calculated for each bound conformation. The trend in binding energies agrees with current experimental data, which implicates the highly conserved TM7 residue Glu287 in ligand recognition. Although a larger and more diverse ligand library needs to be docked for complete validation, we are confident that this study is a necessary first step in explaining antagonist-receptor binding differentials across CCR1 species.

References

[1] Haringman, J. J., Kraan, M. C., Smeets, T. J., Zwinderman, K. H., and Tak, P. P. (2003) *Ann. Rheum. Dis.* **62**, 715–721.

[2] Liang, M., Mallari, C., Rosser, M., Ng, H. P., May, K., Monahan, S., Bauman, J. G., Islam, I., Ghannam, A., Buckman, B., Shaw, K., Wei, G. P., Xu, W., Zhao, Z., Ho, E., Shen, J., Oanh, H., Subramanyam, B., Vergona, R., Taub, D., Dunning, L., Harvey, S., Snider, R. M., Hesselgesser, J., Morrissey, M. M., and Perez, H. D. (2000) *J. Biol. Chem.* **275**, 19000–19008.

[3] Horuk, R., Clayberger, C., Krensky, A. M., Wang, Z., Grone, H. J., Weber, C., Weber, K. S., Nelson, P. J., May, K., Rosser, M., Dunning, L., Liang, M., Buckman, B., Ghannam, A., Ng, H. P., Islam, I., Bauman, J. G., Wei, G. P., Monahan, S., Xu, W., Snider, R. M., Morrissey, M. M., Hesselgesser, J., and Perez, H. D. (2001) *J. Biol. Chem.* **276**, 4199–4204.

[4] Onuffer, J., McCarrick, M. A., Dunning, L., Liang, M., Rosser, M., Wei, G. P., Ng, H., and Horuk, R. (2003) *J. Immunol.* **170**, 1910-1916.

[5] Floriano, W. B., Vaidehi, N., Singer, M., Shepherd, G., and Goddard, W. A. III (2000) *Proc. Natl. Acad. Sci. USA* **97**, 10712-10716.

[6] Vaidehi, N., Floriano, W. B., Trabanino, R., Hall, S. E., Freddolino, P., Choi, E. J., Zamanakos, G., and Goddard, W. A. III (2002) *Proc. Natl. Acad. Sci. USA* **99**, 12622-12627.

[7] Trabanino, R. J., Hall, S. E., Vaidehi, N., Floriano, W. B., Kam, V. W. T., and Goddard, W. A. III (2004) *Biophys. J.* **86**, 1904-1921.

[8] Kekenes-Huskey, P. M., Vaidehi, N., Floriano, W. B., and Goddard, W. A. III (2003) *J. Chem. Phys. B* **107**, 11549-11557.

[9] Datta, D., Vaidehi, N., Zhang, D., and Goddard, W. A. III (2004) *Prot. Sci.* **13**, 2693-2705.

[10] Palczewski, K., Kumasaka, T., Hori, T., Behnke, C., Motoshima, H., Fox, B., Trong, I., Teller, D., Okada, T., Stenkamp, R., Yamamoto, M., and Miyano, M. (2000) *Science* **289**, 739-745.

[11] Freddolino, P. L., Kalani, M. Y., Vaidehi, N., Floriano, W. B., Hall, S. E., Trabanino, R. J., Kam, V., and Goddard, W. A. III (2004) *Proc. Natl. Acad. Sci.* **101**, 2736–2741.

[12] Ewing, T. A., and Kuntz, I. D. (1997) *J. Comput. Chem.* **18**, 1175-1189.

[13] Ng, H. P., May, K., Bauman, J. G., Ghannam, A., Islam, I., Liang, M., Horuk, R., Hesselgesser, J., Snider, R. M., Perez, H. D., and Morrissey, M. M. (1999) *J. Med. Chem.* **42**, 4680-4694.

[14] Zheng, G., Parkin, S., Dwoskin, L. P., and Crooks, P. A. (2004) *Acta Cryst.* **C60**, 9-11.

Table 4-1: Bends and tilts for each helix in mCCR1.

Helix Number	Bend Angle (degrees)	Tilt Angle (degrees)
1	14.8	50.8
2	36.4	19.9
3	3.8	18.7
4	16.3	15.3
5	10.6	24.2
6	13.9	9.5
7	9.1	29.6

Table 4-2: Decomposition of calculated binding energy (-21.81 kcal/mol) for BX471 docked to mCCR1.

Residue (ordered by decreasing total contribution)	vdW Energy (kcal/mol)	Coulomb Energy (kcal/mol)	Total Energy (kcal/mol)
Phe260	-6.11	0.46	-5.64
Tyr114	-4.57	-1.03	-5.60
Phe172	-1.58	-0.13	-1.71
Ala168	-0.81	-0.47	-1.29
Leu109	-1.16	-0.03	-1.19
Tyr113	-0.90	-0.10	-1.00
Tyr291	-0.88	-0.07	-0.96
Phe171	-0.58	-0.21	-0.79
Leu208	-0.79	0.06	-0.74
Ser110	-0.57	-0.12	-0.69
Thr253	-0.29	-0.22	-0.50

Σ = -20.11 kcal/mol

More stable in mCCR1 (lower energy compared to hCCR1)

Less stable in mCCR1 (higher energy compared to hCCR1)

Table 4-3: Correlation between calculated binding energies (BE) and experimental binding affinities (K_i) for mCCR1 docked ligand library.

Ligand	5Å Cavity Energy (kcal/mol)	Ligand Solvation Energy (kcal/mol)	Cavity Energy + Solvation Energy (kcal/mol)	Total Ligand Binding Energy (kcal/mol)	Expt. K_i (Nm)
BX523	-30.21	-3.73	-33.94	-35.15	52
BX511	-26.19	-4.19	-30.38	-31.09	332
BX471	-20.11	-1.39	-21.50	-21.81	380

>sp|P51675|CKR1_MOUSE C-C chemokine receptor type 1 (CCR1).
MEISDFTEAYPTTTEFDYGDSTPCQKTAVRAFGAGLLPPLYSLVFIIGVVGNVLMILVLM
QHRRLQSMTSIYLFNLAVSDLVFLFTLPFWIDYKLKDDWIFGDAMCKLLSGFYYLGLYSE
IFFIILLTIDRYLAIVHAVFALRARTVTLGIITSIITWALAILASMPALYFFKAQWEFTH
RTCSPHFPYKSLKQWKRFQALKLNLLGLILPLLVMIICYAGIIRILLRRPSEKKVKAVRL
IFAITLLFFLLWTPYNLSVFVSAFQDVLFTNQCEQSKHLDLAMQVTEVIAYTHCCVNPII
YVFVGERFWKYLRQLFQRHVAIPLAKWLPFLSVDQLERTSSISPSTGEHELSAGF

Figure 4-1: mCCR1 primary sequence in FASTA format.

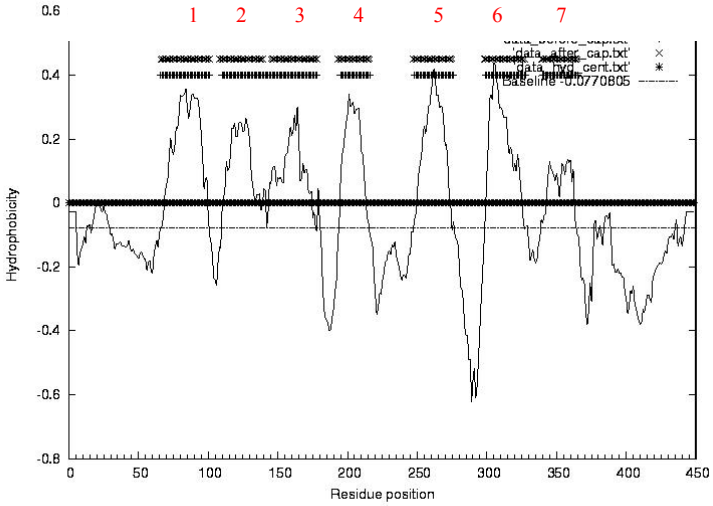

Figure 4-2: mCCR1 hydrophobicity profile.
Indicated in red are TM domains 1-7 at window size 12.

NT:	**1**	MEISDFTEAYPTTTEFDYGDSTPCQKTAVR	
TM1:	**31**	AFGAGLLPPLYSLVFIIGVVGNVLMILVLMQH	**62**
IC1:		RRLQS	
TM2:	**68**	MTSIYLFNLAVSDLVFLFTLPFWIDYKLKDD	**98**
EC1:		WIFGD	
TM3:	**104**	AMCKLLSGFYYLGLYSEIFFIILLTIDRYLAIVH	**137**
IC2:		AVFALRARTVTL	
TM4:	**150**	GIITSIITWALAILASMPALYFFK	**173**
EC2:		AQWEFTHRTCSPHFPYKSLKQW	
TM5:	**196**	KRFQALKLNLLGLILPLLVMIICYAGIIR	**224**
IC3:		ILLRRPSEKKVKAV	
TM6:	**239**	RLIFAITLLFFLLWTPYNLSVFVSVFQDVL	**268**
EC3:		FTNQCEQSKH	
TM7:	**279**	LDLAMQVTEVIAYTHCCVNPIIYVFVG	**305**
CT:		ERFWKYLRQLFQRHVAIPLAKWLPFLSVDRLERTSSISPSTGEHELSAGF	**355**

Figure 4-3: mCCR1 TM regions.
NT = N-terminus, CT = C-terminus, IC = intracellular, and EC = extracellular domains. Highlighted in red are the hydrophobic center predictions for each helix.

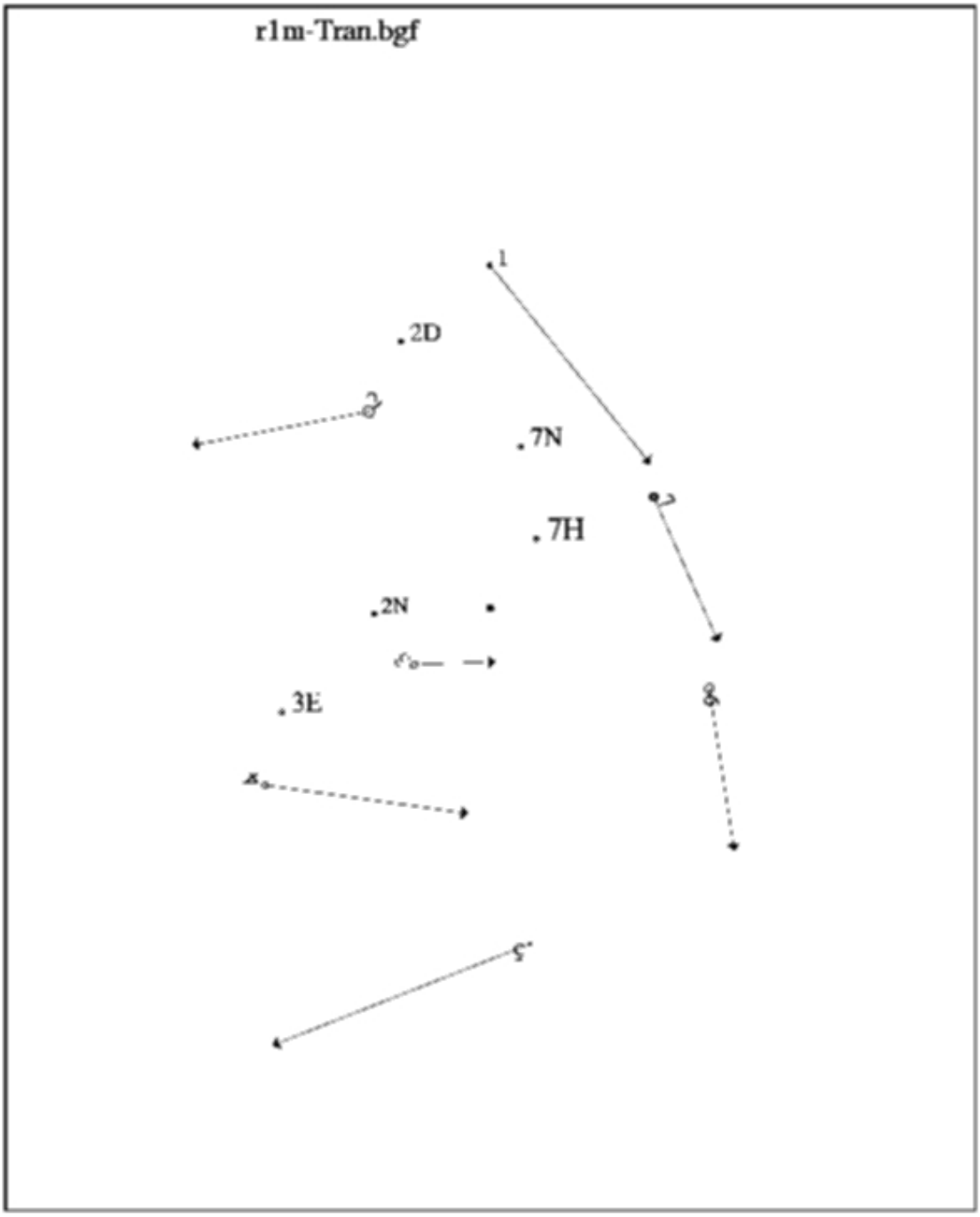

Figure 4-4: mCCR1 bundle before rotational optimization.
The numbers 1-7 refer to the TM regions, and the direction of the arrow indicates the net hydrophobic moment of the helix. Note that the moments are randomly oriented. The lipid membrane, not shown here, is packed uniformly around the bundle.

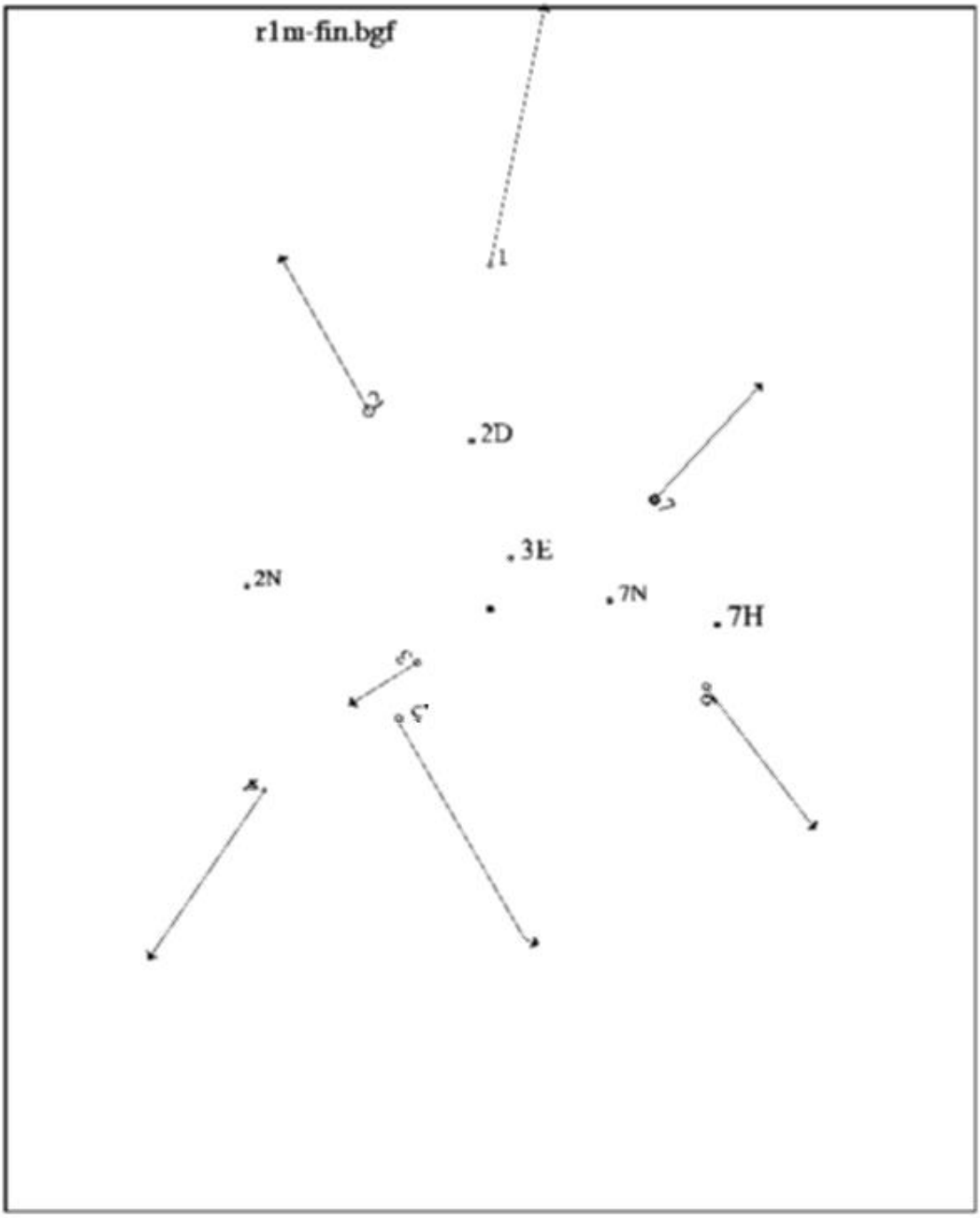

Figure 4-5: mCCR1 bundle after rotational optimization.
After rotational optimization, the hydrophobic moments are now oriented outward, facing the lipid membrane.

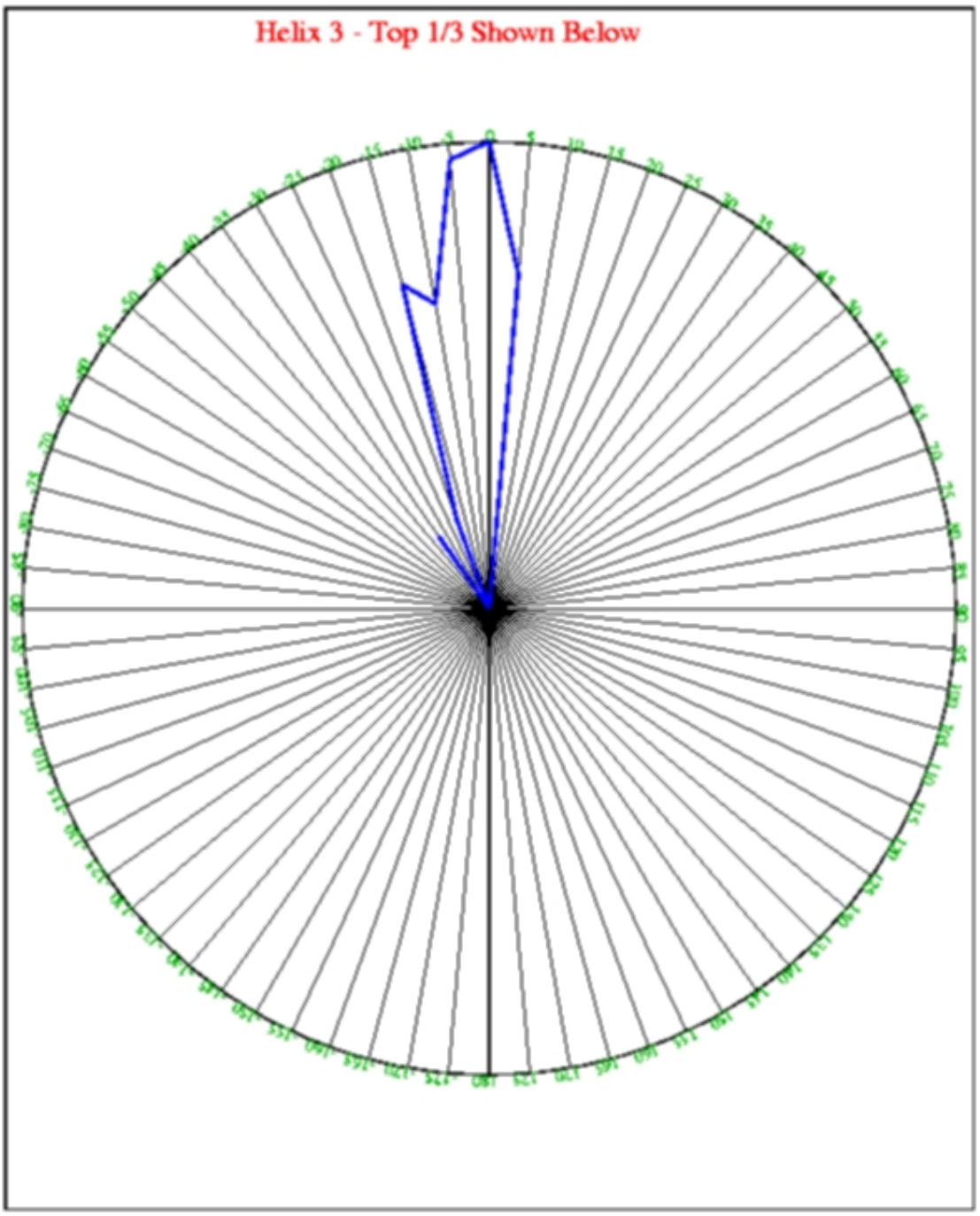

Figure 4-6: mCCR1 TM3 rotational optimization using RotMin.
After conducting a global energy scan for TM3, a minimum at 0° is observed (i.e., no need for further rotational optimization).

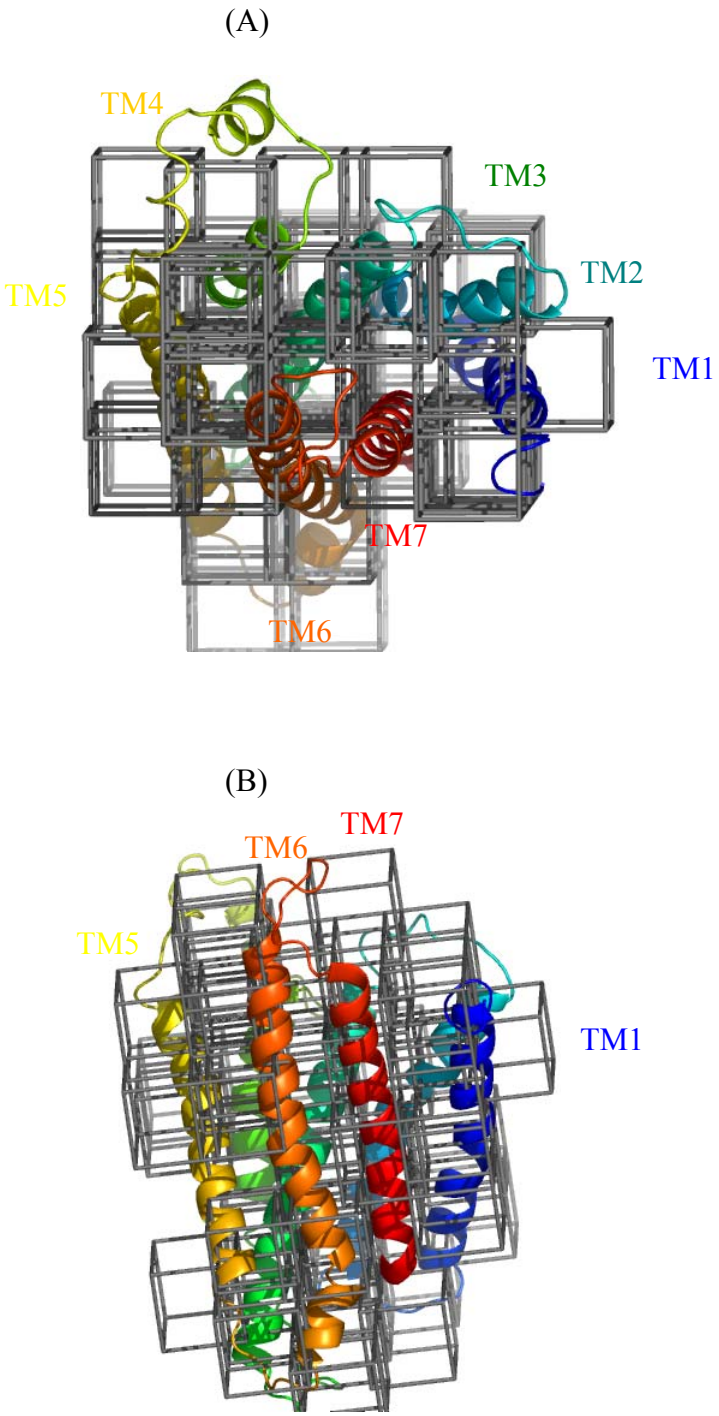

Figure 4-7: mCCR1 putative binding sites.
After scanning the molecular surface of the receptor, 49 boxes (each 1000 $Å^3$) containing a total of 11625 spheres are generated. Shown in (A) is the top view, and (B) the side view. Note the convention used here is the extracellular side on "top" and thus the intracellular interface is below. Also provided is the color code used for helices in the bundle.

(A)

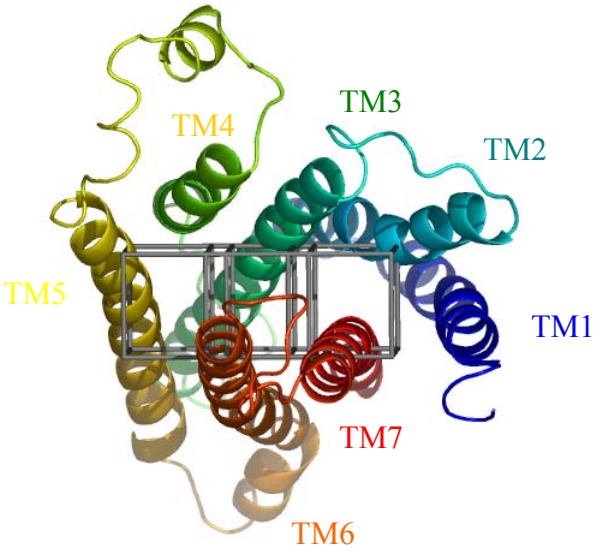

(B)

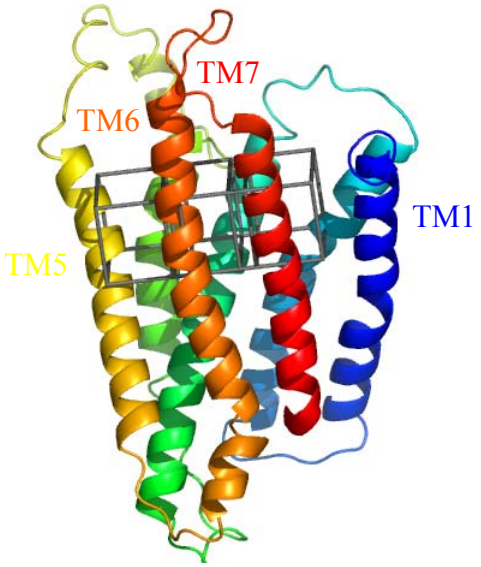

Figure 4-8: mCCR1 binding sites for docking.
From the 49 putative binding sites, we determine our refined binding site to be a horizontal mode across 3 contiguous regions (27, 31, and 32). Shown in (A) is the top view, and (B) the side view.

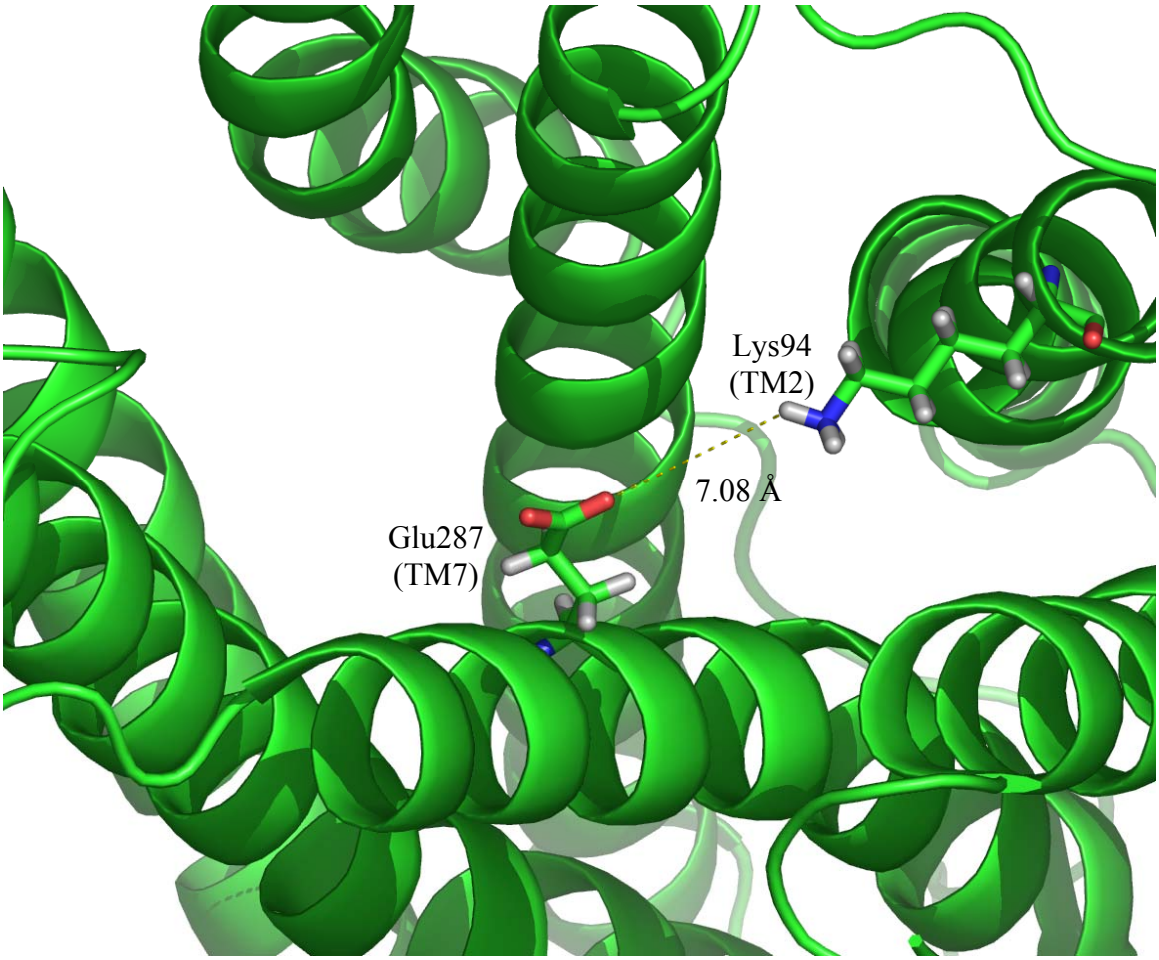

Figure 4-9: mCCR1 salt bridge (TM2-7).
Water mediated salt bridge between Lys94 (TM2) and Glu287 (TM7).

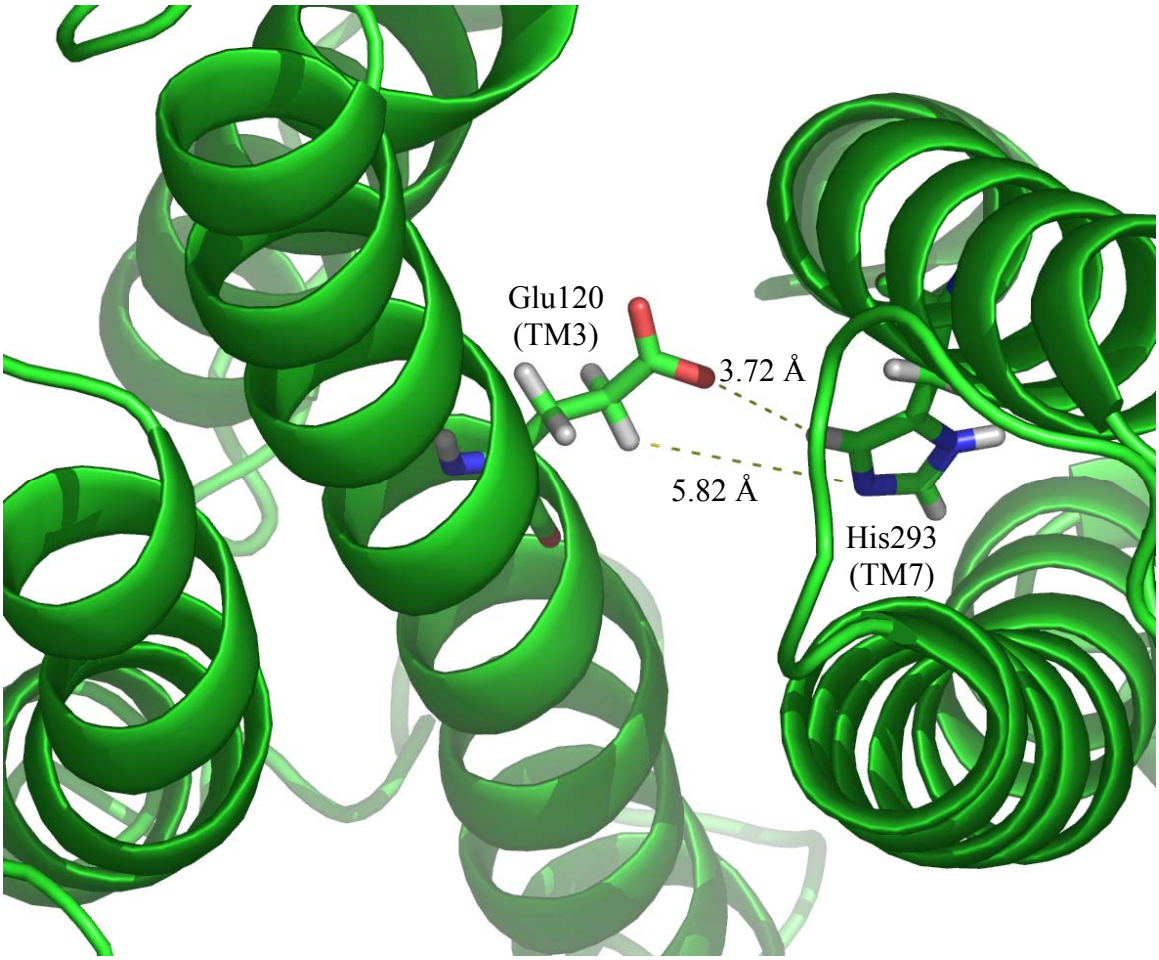

Figure 4-10: mCCR1 salt bridge (TM3-7).
Salt bridge between Glu120 (TM3) and His293 (TM7).

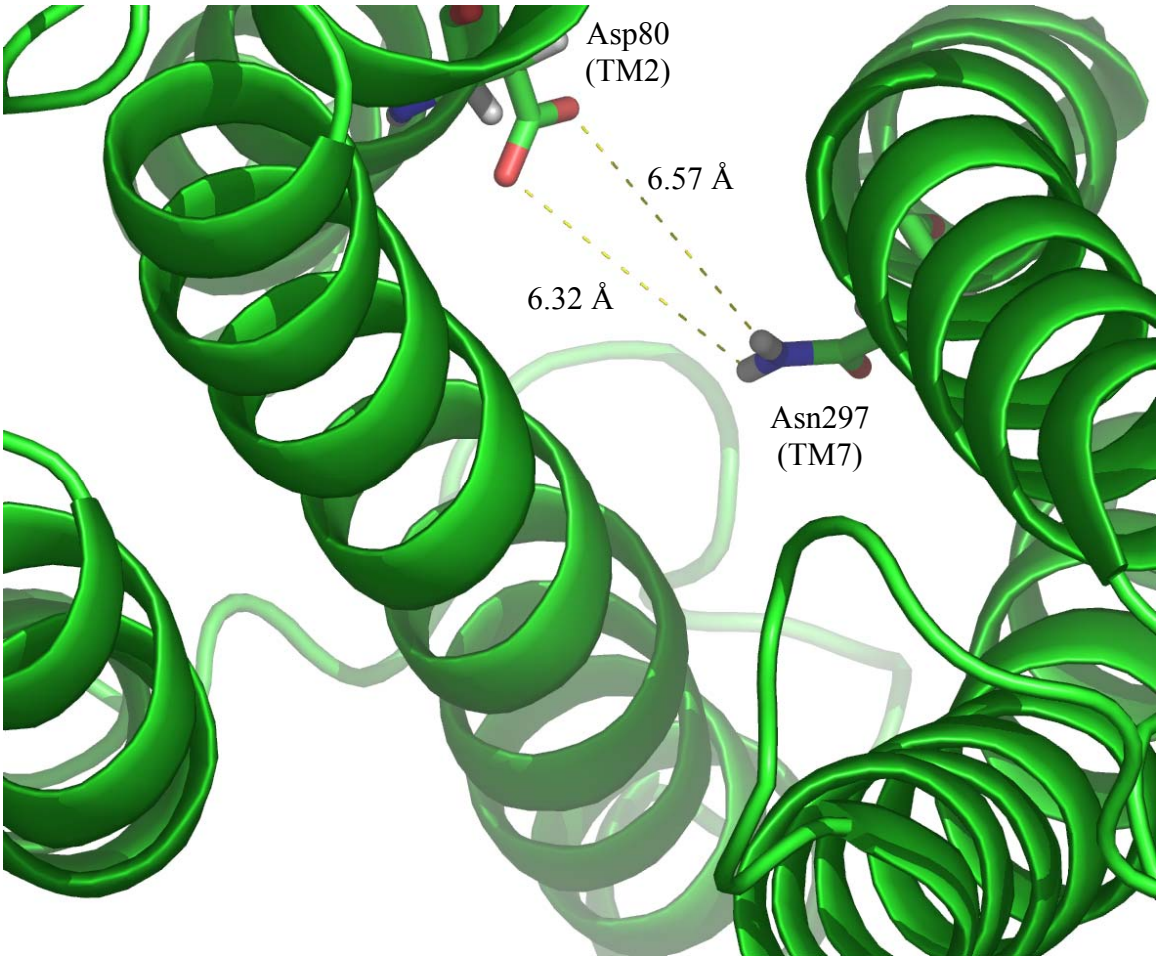

Figure 4-11: mCCR1 inter-helical hydrogen bonding (TM2-7).
Water mediated hydrogen bonds between Asp80 (TM2) and Asn297 (TM7). These are conserved residues across many GPCRs.

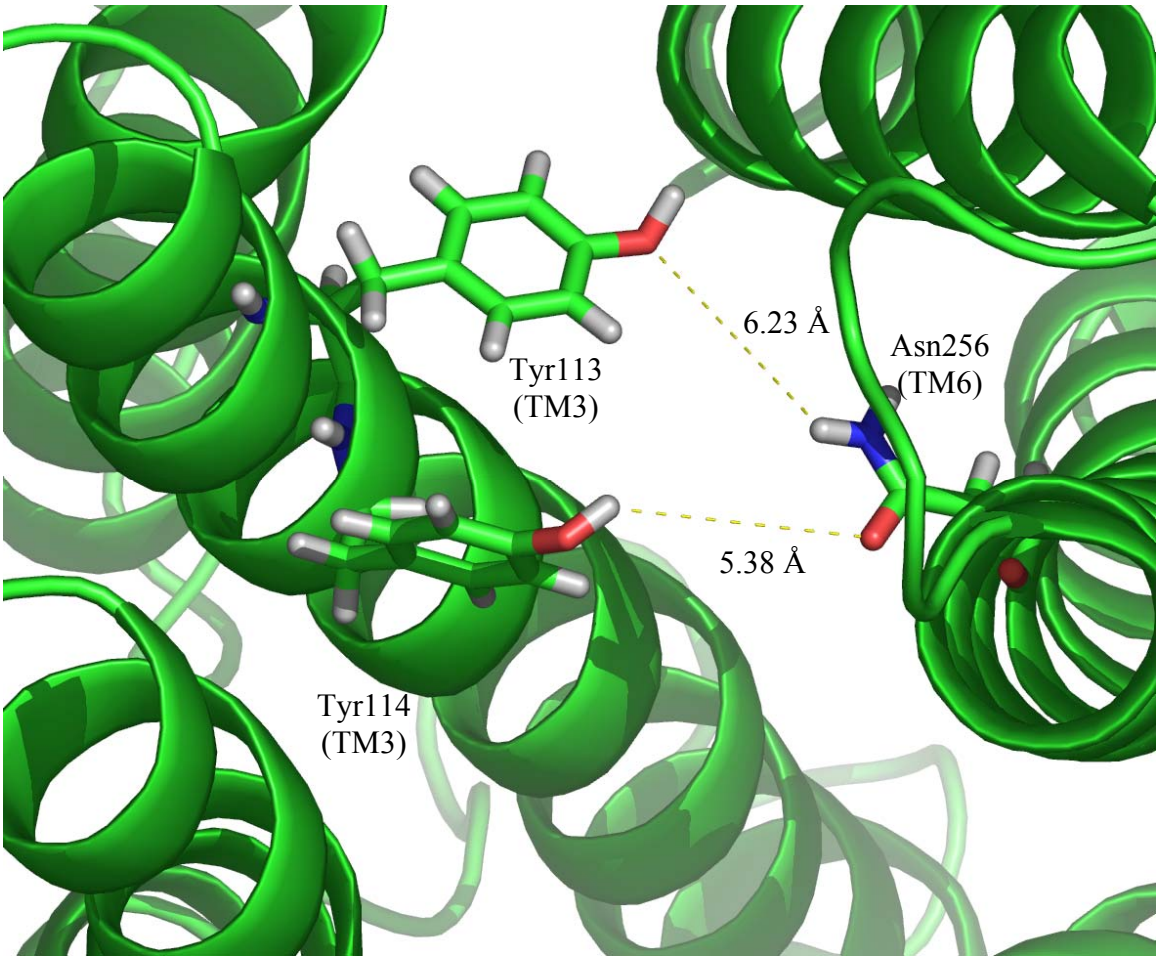

Figure 4-12: mCCR1 inter-helical hydrogen bonds (TM3-6).
Weak hydrogen bonding between Tyr113 (TM3), Tyr114 (TM3), and Asn256 (TM6). Asn256 is part of the WXPFF motif (WTPYN in hCCR1) in biogenic amine GPCRs.

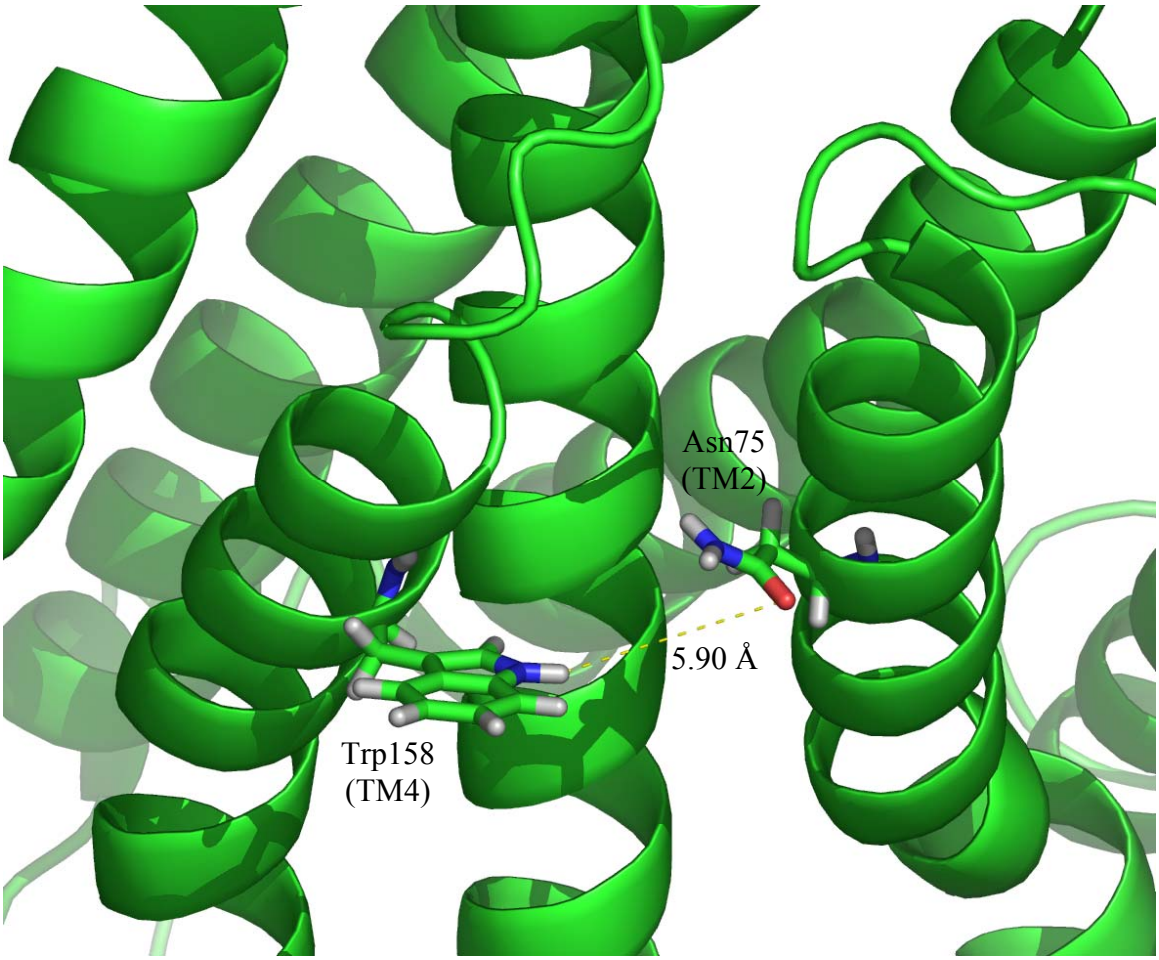

Figure 4-13: mCCR1 inter-helical hydrogen bond (TM2-4).
Hydrogen bond between Asn75 (TM2) and Trp158 (TM4). Trp158 is the most conserved TM4 residue across all GPCRs.

(A)

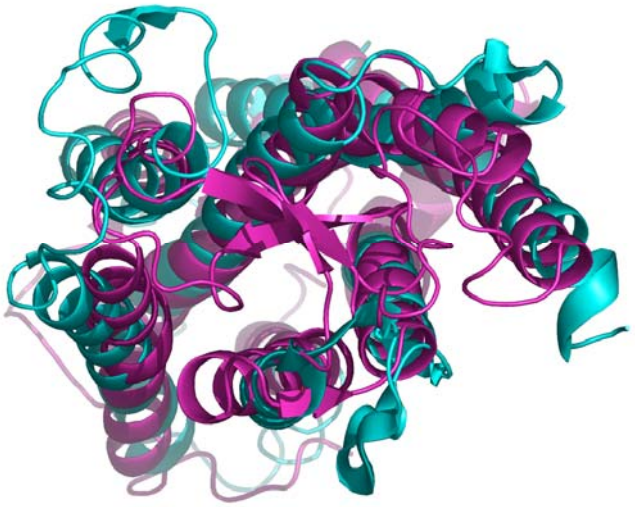

mCCR1

BR

(B)

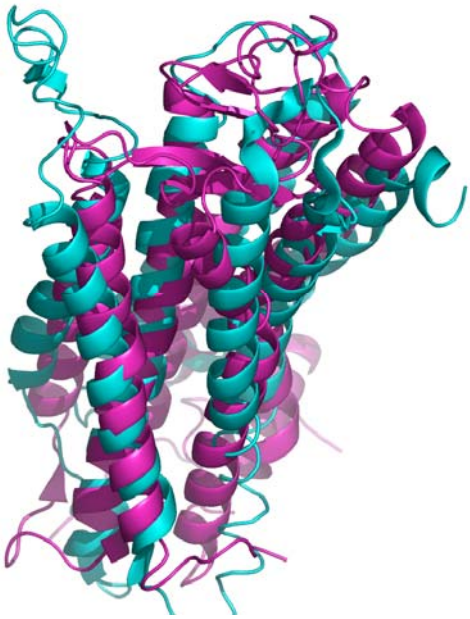

Figure 4-14: Overlay of the mCCR1 and BR structures.
Predicted mCCR1 structure superimposed on experimental BR structure (PDB #1F88). The main chain RMSD is 5.20 Å.

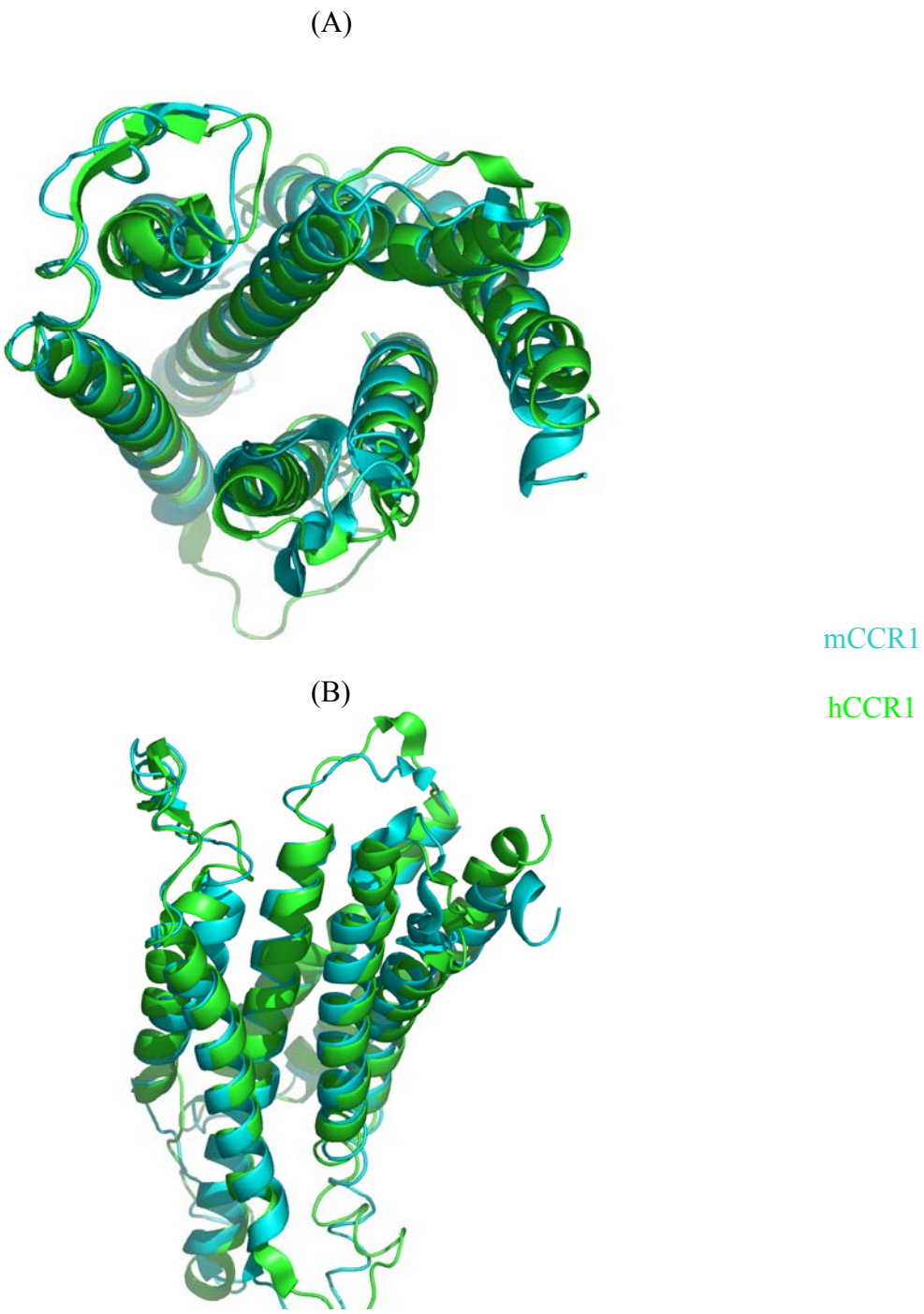

Figure 4-15: Overlay of the mCCR1 and hCCR1 structures.
Predicted mCCR1 structure superimposed on predicted hCCR1 structure. The main chain RMSD is 2.91 Å.

```
CLUSTAL W (1.82) multiple sequence alignment


hCCR1           AFGAQLLPPLYSLVFVIGLVGNILVVLVLVQYMTSIYLLNLAISDLLFLFTLPFWIDYKL 60
mCCR1           AFGAGLLPPLYSLVFIIGVVGNVLMILVLMQHMTSIYLFNLAVSDLVFLFTLPFWIDYKL 60
                **** **********:**:***:*::***:*:******:***:***:**************

hCCR1           KDDAMCKILSGFYYTGLYSEIFFIILLTIDRYLAIVHGVITSIIIWALAILASMPGLYFS 120
mCCR1           KDDAMCKLLSGFYYLGLYSEIFFIILLTIDRYLAIVHGIITSIITWALAILASMPALYFF 120
                *******:****** **********************:***** **********.***

hCCR1           KKLFQALKLNLFGLVLPLLVMIICYTGIIKRLIFVIMIIFFLFWTPYNLTILISVFQD-- 178
mCCR1           KKRFQALKLNLLGLILPLLVMIICYAGIIRRLIFAITLLFFLLWTPYNLSVFVSVFQDVL 180
                ** ********:**:**********:***:****.* ::***:******::::*****

hCCR1           LDLAVQVTEVIAYTHCCVNPVIYAFVG 205
mCCR1           LDLAMQVTEVIAYTHCCVNPIIYVFVG 207
                ****:***************:**.***
```

Figure 4-16: TM sequence alignment of hCCR1 and mCCR1.
Sequence alignment of predicted TM regions of hCCR1 and mCCR1. The identity is 83%; 79% in overall sequence.

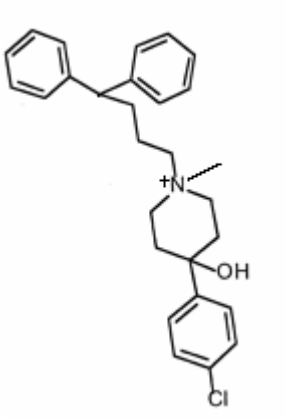

BX523

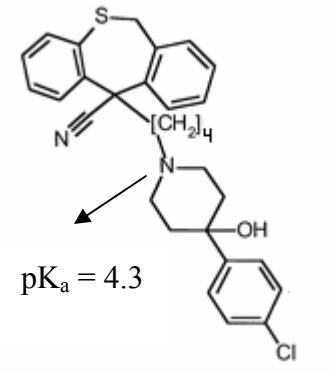

BX511

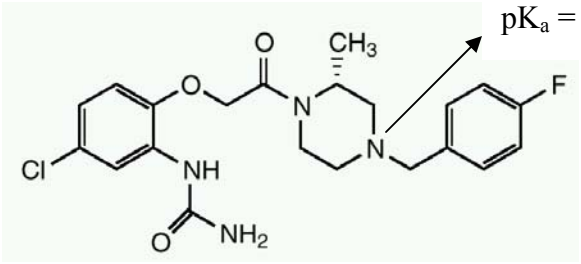

BX471

Figure 4-17: Structures of BX523, BX511, and BX471 antagonists.

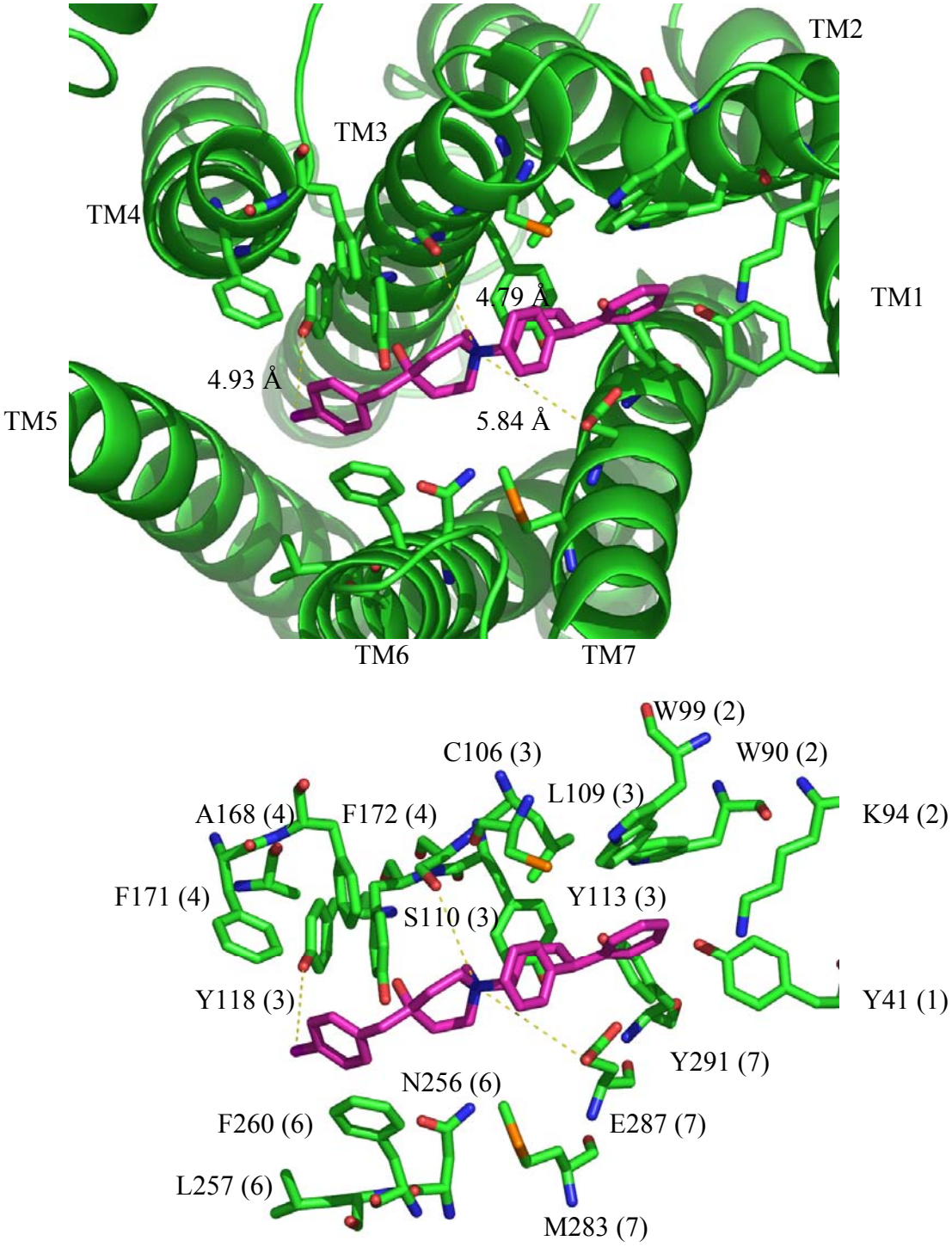

Figure 4-18: Ionic interactions in the 5Å BX523 binding cavity (top).
The ligand is anchored by ionic interactions with Ser110 or Glu287, and Tyr118. The number in parenthesis indicates the helix number, and the distances shown are between heavy atoms.

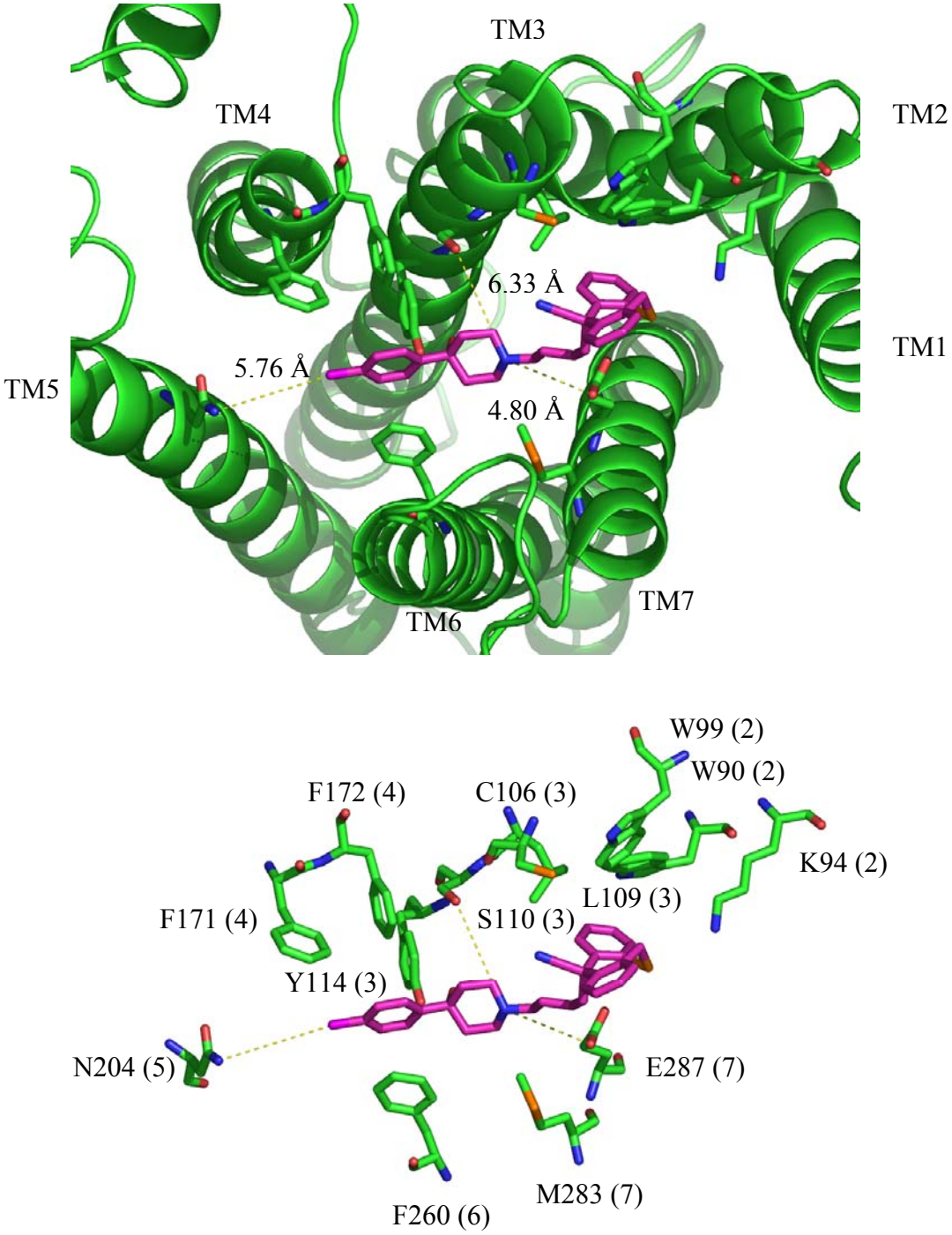

Figure 4-19: Ionic interactions in the 5Å BX511 binding cavity (top).
The ligand is anchored by ionic interactions with Ser110 or Glu287, and Asn204.

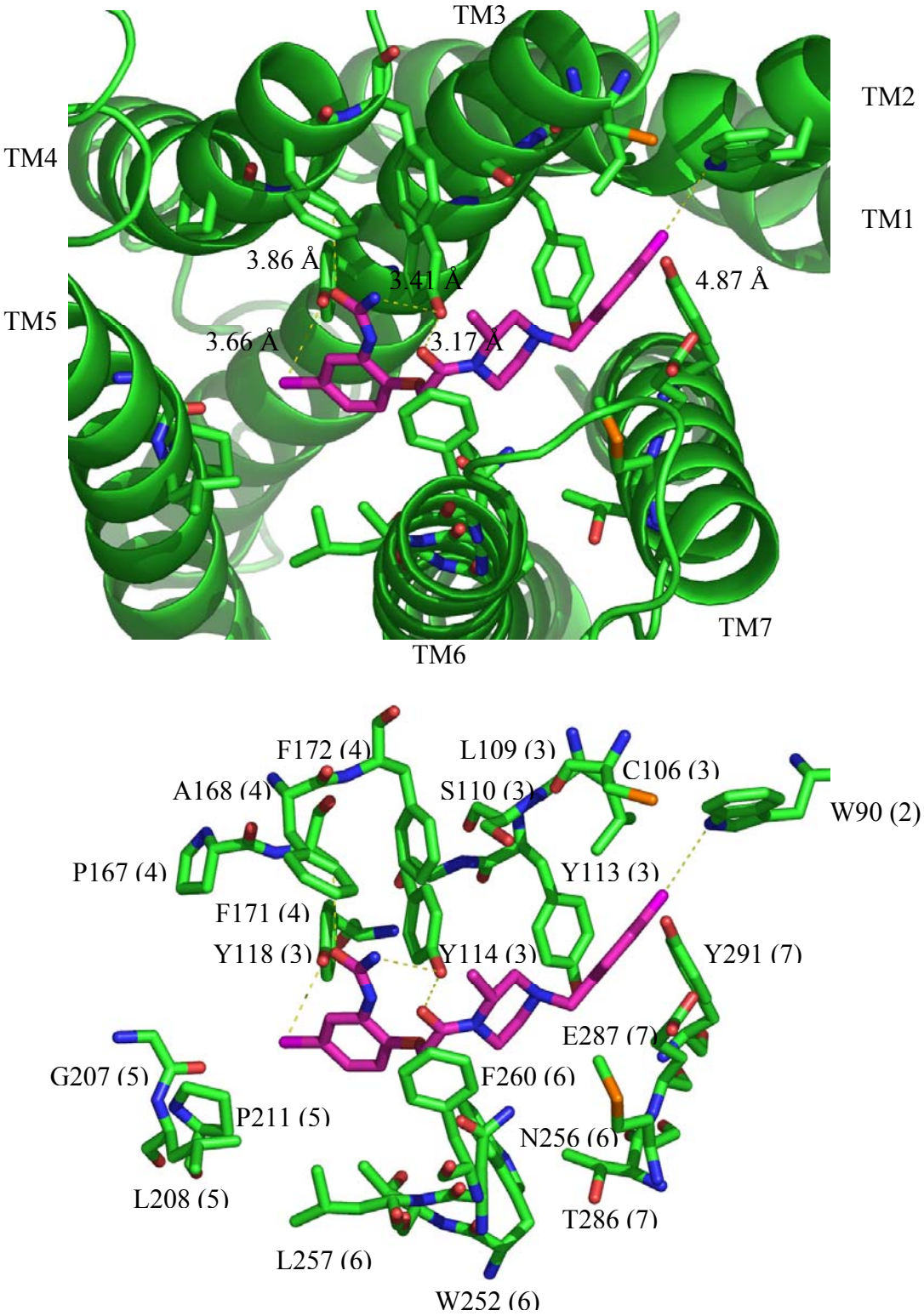

Figure 4-20: Ionic interactions in the 5Å BX471 binding cavity (top).
The ligand is anchored by ionic interactions with Ala168, Tyr114, Ser110, and Tyr291. The magnitude of these interactions is quantified in Table 4-2.

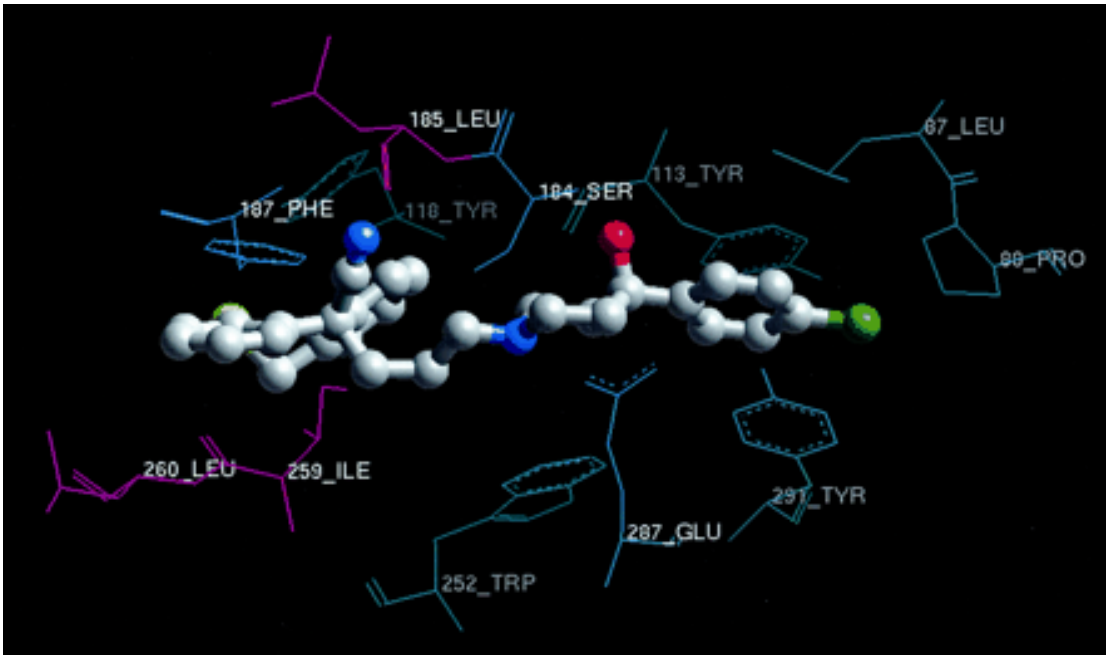

Figure 4-21: Binding mode of BX510 in hCCR1 homology model.
BX510 (shown) is structurally similar to BX511 (Figure 4-19), although we observe an inverted binding mode. Glu287 (TM7) is in our binding site. Reproduced with permission from Onuffer, et al., (2003) *J. Immunol.* **170**, 1910-1916.